PERGAMON

Aerosol Science 34 (2003) 1371–1397

Journal of
Aerosol Science

www.elsevier.com/locate/jaerosci

COSIMA—a computer program simulating the dynamics of fractal aerosols

Karl-Heinz Naumann*

Forschungszentrum Karlsruhe GmbH, Institut für Meteorologie und Klimaforschung, Postfach 3640, D-76021 Karlsruhe, Germany

Received 4 October 2001; accepted 21 December 2002

Abstract

The sectional aerosol behavior code COSIMA simulates the time evolution of the structural, dynamical, and optical properties of airborne agglomerate particles as well as their heterogeneous chemical interactions with reactive trace gases utilizing a formalism based on fractal scaling laws. The modeled processes include diffusion to the walls and sedimentational deposition, Brownian and gravitational coagulation, molecular transport from the gas phase to the accessible particle surface, surface adsorption and reactions, gas phase reactions, and dilution effects due to sampling (e.g. during aerosol chamber experiments). The effect of hydrodynamic interactions and shielding on particle mobility is considered within the framework of the Kirkwood–Riseman theory. Rayleigh–Debye–Gans theory is used to deal with light absorption and scattering. The code is validated against new experimental data on the dynamics of Diesel and graphite spark soot as well as recent theoretical and simulation results. Applying the Kirkwood–Riseman formalism to compute the mobility of fractal like agglomerates significantly enhances coagulation rates as well as wall and depositional loss but does not affect the form of the self preserving size distributions attained in the long time regime if Brownian coagulation dominates the aerosol dynamics.

1. Introduction

Solid aerosol particles generated by combustion or plasma processes often exhibit ramified, apparently irregular agglomerate structures. Their optical and dynamical properties differ significantly from those of compact spherical species. Consequently, tools like Mie theory (Bohren & Huffman, 1998) and standard type aerosol behavior codes (Seigneur et al., 1986; Zhang, Seigneur, Seinfeld, Jacobson, & Binkowski, 1999) are not directly applicable for predictive or analytical purposes. This

* Tel.: +49-7247-823941; fax: +49-7247-823943.
E-mail address: karl-heinz.naumann@imk.fzk.de (K.-H. Naumann).

0021-8502/$ - see front matter © 2003 Elsevier Ltd. All rights reserved.
doi:10.1016/S0021-8502(03)00367-7

Nomenclature

a	exponent in size dependence of diffusive boundary layer thickness
A	constant in slip correction formula
A_{D}	diffusional deposition area
A_{S}	sedimentational deposition area
b	constant in slip correction formula
$B(R_0)$	mobility of isolated primary particles
c_{m}	mass concentration
c_{n}	number concentration
c_{v}	volume concentration
$c(r)$	radial density distribution of monomers in fractal particles
d_{f}	volume fractal dimension
d_{s}	surface fractal dimension
D	translational diffusion coefficient
D_0	unit translational diffusion coefficient in Eq. (40)
$D(R_{\mathrm{me},k})$	translational diffusion coefficient for section k
f	volume filling factor
g	gravitational acceleration
$g(r)$	radial pair distribution function of monomers in fractal particles
$g(\lambda, \langle R_{\mathrm{g}}^2 \rangle, d_{\mathrm{f}})$	scattering factor
G_{ij}	transition regime interpolation factor for Brownian coagulation
$h(r)$	cut-off term in radial pair distribution function
h_{KR}	Kirkwood–Riseman ratio $R_{\mathrm{me}}/R_{\mathrm{geo}}$
J	transport rate of gas phase molecules to accessible particle surface
k	Boltzmann constant
k_{g}	fractal prefactor
k_{D}	prefactor in size dependence of diffusive boundary layer thickness
k_{p}	wave number$=2\pi/\lambda$
K_{ij}	total coagulation kernel
K_{ij}^{B}	Brownian coagulation kernel
K_{ij}^{G}	gravitational coagulation kernel
Kn_0	Knudsen number of primary particles
l	mean free path of carrier gas molecules
m	particle mass
m_k	particle mass in section k
n	complex refractive index
$n(R_{\mathrm{m},k}, t)$	particle number density in section k
N	number of monomers in a cluster
N_{s}	number of sections used for size discretization
p	pressure
Q	constant in slip correction formula

Nomenclature (*Continued*)

r	distance
r^*	r/R_0
r_p	mean radius in lognormal distribution
R_0	radius of primary particles
R_acc	accessible surface equivalent radius
R_ae	aerodynamic radius
R_eff	effective radius to be used with slip correction
R_geo	geometric radius of fractal particles
R^*_geo	R_geo/R_0
r_{ij}	distance between primary particles i and j
R_m	mass equivalent radius
$R_{\mathrm{m},k}$	mass equivalent radius for section k
R_me	mobility equivalent radius
$R_\mathrm{me,c}$	continuum regime mobility equivalent radius
$R_{\mathrm{me},k}$	mobility equivalent radius for section k
S_acc	accessible particle surface
$S_k(t)$	particle source rate for section k
$S(q)$	structure factor
t	time
T	absolute temperature
v_i	particle volume for section i
V	aerosol chamber volume
x	scaling exponent in Eq. (25)
x_p	$2\pi R_0/\lambda$
z	scaling factor in Eq. (26)
$\alpha^\mathrm{D}_k(t)$	diffusional deposition coefficient for section k
$\alpha^\mathrm{S}_k(t)$	sedimentational deposition coefficient for section k
$\alpha^\mathrm{D}_k(t)$	loss coefficient for section k
β^k_{ij}	interpolation factor for non-mass equidistant size discretization
γ	scaling exponent in Eq. (26)
δ_D	diffusional boundary layer thickness
$\delta_{I,k}$	Kronecker delta
ε_{Ij}	gravitational coagulation efficiency
η	gas viscosity
η_I	dimensionless particle volume for section i
$\Gamma(..)$	gamma function
κ	interpolation factor between gravitational coagulation efficiency limits
λ	wavelength of light
ρ	material density of primary particles
ρ_0	material density of reference particles in Eq. (31)
$\Psi(v_k,t)$	dimensionless particle density function

Nomenclature (*Continued*)

σ	standard deviation in lognormal size distribution
σ_{abs}	specific absorption cross section
σ_{sca}	specific scattering cross section
ξ	scaling factor in Eq. (14)
ξ^*	ξ/R_0

poses a severe problem since agglomerate aerosols are quite abundant in both natural and technical environments. Reacting to this scientific challenge much work has recently been conducted towards a better understanding of the structural, dynamical, and optical properties of agglomerate particles.

It has been well established by now that the volume structure of ramified solid particles is often determined by self-similarity over several orders of magnitude in size (Avnir, 1989; Weitz & Oliveria, 1984; Colbeck & Wu, 1994; Sorensen & Feke, 1996). Therefore, the Hausdorff dimension ("fractal" dimension) d_f (Mandelbrodt, 1982) plays a central role for the geometrical and aerodynamical characterization of such particles. In a statistical sense fractal geometry implies structural irregularity as a normal situation and ideality as limiting case. Combined with statistical mechanics the implementation of fractal scaling laws thus provides a powerful mathematical formalism for the modelling of agglomerate dynamics and optics. The aerosol behavior code COSIMA (COmputer SIMulation of Aerosols) which will be presented in the following has been developed within this framework.

The physical and chemical processes modelled by COSIMA include particle diffusion, sedimentation, coagulation, dilution effects due to sampling (e.g. during aerosol chamber experiments), gas-to-surface transport, surface adsorption, and heterogeneous surface chemistry as well as homogeneous reactions in the gas phase. Regarding the optical properties light absorption and scattering are calculated as a function of time depending on the evolution of the particle size distribution. The code was validated and parameterized by comparing simulated and experimentally determined time evolutions of mass and number concentrations and of size distributions for Diesel soot, soot generated by spark discharge between graphite electrodes, acetylene soot, and uranium dioxide aerosol. During extensive aerosol chamber studies of reactive trace gas interactions with soot particles it was successfully applied to account for the effects of aerosol dynamics on the chemical reaction system and to extract heterogeneous reaction probabilities from the measured gas concentration vs. time profiles (Kamm, Möhler, Naumann, Saathoff, & Schurath, 1999; Saathoff et al., 2001).

2. Fractal formalism

The concept of COSIMA is based on the definition of certain types of effective radii which characterize the structural and dynamical properties of fractal like agglomerates. This allows to formulate the general dynamic equation for collectives of irregularly shaped particles in a manner very similar to the case of compact spherical species. In the following it is assumed that all fractal clusters consist of non-overlapping spherical monomers of equal size (for an approximate extension to

the case of overlapping primary particles see Wentzel, Gorzawski, Naumann, Saathoff, and Weinbruch (2003)). Furthermore the radial density distribution of the monomers is assumed to be spherically isotropic, i.e. a possible angular dependence of the density distribution is neglected. This clearly restricts the validity of the presented formalism to fractal dimensions d_f well above 1. An arbitrarily constructed fractal with $d_f = 1$ can exhibit a connected structure only if projected onto one axis. In the case of an agglomerate consisting of spherical monomers this corresponds to a straight non-branched chain. Every attempt to transform such a chain into a spherically symmetric three-dimensional density distribution will inevitably result in breaking of all bonds. From this it necessarily follows that agglomerate particles will assume increasingly anisotropic forms when approaching the limiting case $d_f = 1$. However, the degree of particle anisotropy is not only a function of the fractal dimension but depends also on the kind of processes dominating the formation and growth of the particles (Meakin, 1998; Botet & Jullien, 1986; Kolb, 1985; Meakin & Vicsek, 1985). The structure of simulated clusters generated by diffusion limited cluster–cluster aggregation (DLCCA) (Mountain & Mulholland, 1988) often closely resembles that of airborne agglomerates. This growth process has been found to yield angularly isotropic particles (Kolb, 1985), in contrast to the theoretical reasoning by Botet and Jullien (1986). In practice translational particle motion is always accompanied by rotational Brownian diffusion, resulting in a certain amount of orientational averaging as far as particle dynamics are concerned. Since the fractal dimension d_f of DLCCA clusters is around 1.8, the assumption of spherical isotropy should therefore be acceptable at least for the regime $1.8 < d_f < 3.0$ which comprises most cases of practical interest.

2.1. Geometrical radius and radius of gyration

The effective geometrical radius R_{geo} of a fractal particle is defined here as the radius of its closest convex envelope. This quantity provides the information about the collisional cross section which is required to calculate coagulation rates. To derive a relation between R_{geo} and d_f it is convenient to utilize the radial density distribution function $c(r)$, which is a measure for the probability that a monomer can be found at a distance r from the center of the cluster. The asymptotic form for $c(r)$ is given by (Naumann & Bunz, 1991; Rosner & Tandon, 1994)

$$c(r) = \frac{d_f}{3}\, r^{d_f - 3}. \tag{1}$$

Neglecting a correction term to $c(r)$ that accounts for deviations from the asymptotic form when r is of the order of $2R_0$ the mass of a particle with geometrical radius R_{geo} can be written as

$$m(R_{geo}) = \frac{4\pi\rho R_0^3}{f} \int_0^{R^*_{geo}} c(r^*) r^{*2}\, \mathrm{d}r^* = \frac{4\pi\rho R_0^3}{3f}\, R^{*d_f}_{geo}. \tag{2}$$

The volume filling factor f accounts for the fact that even in a most closely packed structure the spherical monomers can occupy only about 74% of the available volume. The radius of the mass equivalent compact particle is

$$R_m = \left[\frac{3m(R_{geo})}{4\pi\rho}\right]^{1/3}. \tag{3}$$

By comparing Eqs. (2) and (3) one arrives at

$$\frac{R_{geo}}{R_0} = \left[f \left(\frac{R_m}{R_0} \right)^3 \right]^{1/d_f}. \tag{4}$$

Noting that $(R_m/R_0)^3 = N$, the number of primary particles constituting the agglomerate, leads to the equivalent expression

$$\frac{R_{geo}}{R_0} = (fN)^{1/d_f}. \tag{5}$$

Using completely different arguments Eq. (4) has first been derived by Schmidt-Ott (1988a, b). To achieve consistency of his result with the route presented above the pre-factor $d_f/3$ has to be included into the expression for $c(r)$, Eq. (1), which is very often neglected in the literature.

Another important property related to the structural as well as the optical properties of fractal-like particles is the radius of gyration, R_g. It is given by (van Saarloos, 1987)

$$\frac{R_g}{R_0} = \left(\frac{\int_0^{R^*_{geo}} c(r^*) r^{*4} \, dr^*}{\int_0^{R^*_{geo}} c(r^*) r^{*2} \, dr^*} \right)^{1/2} = \sqrt{\frac{d_f}{d_f + 2}} \frac{R_{geo}}{R_0}. \tag{6}$$

Eqs. (5) and (6) provide a simple recipe for the estimation of the pre-factor k_g in the well known scaling relation $N = k_g \, (R_g/R_0)^{d_f}$:

$$k_g = \frac{1}{f} \left[\frac{d_f}{d_f + 2} \right]^{-d_f/2}. \tag{7}$$

The value to be used for k_g has been subject to substantial controversy in the recent literature (see e.g. Brasil, Farias, & Carvalho, 2000; Sorensen & Roberts, 1997; Dobbins, Mulholland, & Bryner, 1994; Wu & Friedlander, 1993a; Sorensen, Cai, & Lu, 1992). Assuming $f = 1.43$, i.e. close to the densest packing limit, for optimum consistency between experimental and simulation results (Naumann & Bunz, 1991; Nyeki & Colbeck, 1994) Eq. (7) predicts k_g to 1.37 for $d_f = 1.82$, in good agreement with the values reported by Wu and Friedlander (1993a) and more recently by Sorensen and Roberts (1997) for DLCCA clusters.

2.2. Accessible surface and mobility equivalent radius

Except for the case of closely packed agglomerates the mobility equivalent radius R_{me} of fractal particles will more or less differ from the geometrical radius R_{geo} (Filippov, 2000; Wang & Sorensen, 1999; Rogak & Flagan, 1989; Chen, Weakliem, & Meakin, 1988). This is due to hydrodynamic interactions between the primary particles, which result in a decrease of the frictional forces acting upon the particles accompanied by an increase of the translational diffusion coefficient (Happel & Brenner, 1963). A rigorous analytical treatment of this effect is restricted to clusters consisting of few monomers with a well defined structure (Happel & Brenner, 1963). For larger particles it is much more efficient to employ statistical–mechanical methods that do not require any structural information beyond the knowledge of the radial pair distribution function $g(r)$ of the monomers. For the continuum regime ($Kn_0 = l/R_0 \to 0$) the Kirkwood–Riseman (KR) theory

(Kirkwood & Riseman, 1948; Doi & Edwards, 1986) provides a useful starting point into this direction (Wiltzius, 1987; Naumann & Bunz, 1991). Although the KR treatment is not rigorously exact, its predictions are usually accurate to better than 10% (Zwanzig, 1966). Then, by generalizing a concept proposed by Dahneke (1973a–c; 1982) for compact non-spherical particles the formalism may be extended to cover the transition and free molecular regimes, too.

Following Kirkwood and Riseman, the translational diffusion coefficient D of a cluster consisting of N monomers is given by

$$D = kTB(R_0)\left[\frac{1}{N} + \left\langle \frac{R_0}{r_{ij}} \right\rangle\right] \tag{8}$$

with $\langle\,\rangle$ denoting statistical averaging. Assuming Stokes' flow in a medium of viscosity η, Eq. (8) takes the form

$$D = \frac{kT}{6\pi\eta}\left[\frac{1}{NR_0} + \left\langle \frac{1}{r_{ij}} \right\rangle\right]. \tag{9}$$

By comparison with the well-known Stokes' formula

$$D = \frac{kT}{6\pi\eta R_{\mathrm{me}}} \tag{10}$$

the KR result for the mobility equivalent radius R_{me} is obtained:

$$\frac{1}{R_{\mathrm{me}}} = \frac{1}{NR_0} + \left\langle \frac{1}{r_{ij}} \right\rangle. \tag{11}$$

For most practical purposes the $1/NR_0$-term can be neglected since it is usually small compared to $\langle 1/r_{ij}\rangle$. Significant contributions are to be expected for small sized clusters and/or for agglomerates with low fractal dimensionality. However, both cases will not be considered within the context of this paper for reasons discussed above. For spherically symmetric agglomerates the average of the inverse monomer distance is related to the radial pair distribution function $g(r)$ of the monomers by

$$\left\langle \frac{1}{r_{ij}} \right\rangle = \frac{\int_{2R_0}^{\infty} r g(r)\,\mathrm{d}r}{\int_{2R_0}^{\infty} r^2 g(r)\,\mathrm{d}r}. \tag{12}$$

The asymptotic form for $g(r)$ is

$$g(r) = \frac{d_{\mathrm{f}}}{3}\, r^{d_{\mathrm{f}}-3} h(r) \tag{13}$$

with $h(r)$ representing the cut-off function. Except for small clusters consisting of only a few monomers a correction term to Eq. (13) accounting for short range order effects can be neglected when evaluating the integrals in Eq. (12). In the following, Eq. (13) is assumed to be valid for all distances r. Furthermore, the lower integration limits are taken as 0 instead of $2R_0$ in order to facilitate analytical solutions.

Calculated values for R_{me} are quite sensitive to the form chosen for the cut-off function $h(r)$. Several approximate expressions for $h(r)$ are in use and have been discussed in the literature (see e.g. Sorensen, 2001; Botet, Rannou, & Cabane, 1995; Cai, Lu, & Sorensen, 1995; Yanwei & Meriani, 1994). Already the crudest approximations, step cut-off and exponential cut-off, lead to meaningful

results when used to estimate fractal parameters from measured mobility equivalent or aerodynamic radii within the KR framework (Naumann & Bunz, 1991; Nyeki & Colbeck, 1994). Much closer to reality, however, is the Gaussian cut-off (Cai et al., 1995; Yanwei & Meriani, 1994; Naumann, to be published)

$$h(r) = \exp\left(-\frac{r^2}{\xi^2}\right) \tag{14}$$

which results in the following analytical solution for R_{me}:

$$R_{\mathrm{me}} = \frac{\xi\Gamma(d_{\mathrm{f}}/2)}{\Gamma((d_{\mathrm{f}}-1)/2)}. \tag{15}$$

The value of the scaling parameter ξ depends on the fractal dimension d_{f} and is of the order of magnitude of R_{geo}. It is uniquely determined due to the fact that the mass of a fractal particle is related to $g(r)$ by

$$m = \frac{4\pi\rho R_0^3}{f} \int_0^\infty r^{*2} g(r^*)\,\mathrm{d}r^*. \tag{16}$$

Inserting Eq. (13) for $g(r)$ together with Eq. (14) yields (with $\xi^* = \xi/R_0$)

$$m = \frac{4\pi\rho R_0^3 d_{\mathrm{f}}}{3f} \int_0^\infty r^{*d_{\mathrm{f}}-1} \exp\left(-\frac{r^{*2}}{\xi^{*2}}\right) \mathrm{d}r^* = \frac{2\pi\rho R_0^3}{3f}\, d_{\mathrm{f}} \xi^{*d_{\mathrm{f}}} \Gamma\left(\frac{d_{\mathrm{f}}}{2}\right). \tag{17}$$

Comparing this result with Eq. (2) leads to

$$\xi = R_{\mathrm{geo}} \left[\frac{2}{d_{\mathrm{f}}\Gamma(d_{\mathrm{f}}/2)}\right]^{1/d_{\mathrm{f}}}. \tag{18}$$

Eq. (18) predicts ratios ξ/R_{geo} equal to 1 and 0.9095 for $d_{\mathrm{f}} = 2$ and 3, respectively, indicating a slight violation of the requirement $g(r) \to 0$ as $r \to 2R_{\mathrm{geo}}$. Nevertheless $g(r)$ decays rapidly enough to warrant using infinity as upper integration limit in Eqs. (12), (16) and (17).

For clusters exhibiting an ideal spherical-symmetrical density distribution as defined by Eq. (1) the following exact expression for $h(r)$ has been derived (Naumann, to be published):

$$h(r) = \frac{1}{2} + \frac{d_{\mathrm{f}}}{2(d_{\mathrm{f}}-1)} \frac{R_{\mathrm{geo}}}{r} - \frac{d_{\mathrm{f}}}{4(d_{\mathrm{f}}-1)} \frac{r}{R_{\mathrm{geo}}} - \frac{(1 - r/R_{\mathrm{geo}})^{d_{\mathrm{f}}}}{2(d_{\mathrm{f}}^2-1)} \left(1 + \frac{R_{\mathrm{geo}}}{r} d_{\mathrm{f}}\right), \quad 0 \leqslant r \leqslant R_{\mathrm{geo}}, \tag{19a}$$

$$h(r) = \frac{1}{2} + \frac{d_{\mathrm{f}}}{2(d_{\mathrm{f}}-1)} \frac{R_{\mathrm{geo}}}{r} - \frac{d_{\mathrm{f}}}{4(d_{\mathrm{f}}-1)} \frac{r}{R_{\mathrm{geo}}} + \frac{(r/R_{\mathrm{geo}} - 1)^{d_{\mathrm{f}}}}{2(d_{\mathrm{f}}^2-1)} \left(1 + \frac{R_{\mathrm{geo}}}{r} d_{\mathrm{f}}\right), \quad R_{\mathrm{geo}} \leqslant r \leqslant 2R_{\mathrm{geo}}. \tag{19b}$$

Please note that in the limiting case $d_f = 3$ the well-known result

$$g(r) = 1 - \frac{3}{4}\frac{r}{R_{geo}} + \frac{1}{16}\left(\frac{r}{R_{geo}}\right)^3, \quad 0 \leqslant r \leqslant 2R_{geo} \tag{20}$$

is recovered from Eqs. (13) and (19). Combining Eqs. (13) and (19) with Eq. (12), closed analytical solutions are only possible for some special values of d_f. For arbitrary fractal dimensions it is necessary to compute R_{me} numerically. In order to obtain a useful working expression, the analytical and numerical results have been fitted to a convenient mathematical form:

$$R_{me} = h_{KR}R_{geo} = (-0.06483d_f^2 + 0.6353d_f - 0.4898)R_{geo}. \tag{21}$$

Inspecting Eqs. (15) and (21) one immediately notes that the ratio R_{me}/R_{geo} (or equivalently the ratio R_{me}/R_g) is predicted to be a function of the fractal dimension only, independent of the particle size. The same holds true for step and exponential cut-off (Naumann & Bunz, 1991; Wang & Sorensen, 1999). This finding is in accord with the results of recent computer simulation studies for particles with fractal dimensions around 1.8 (Rogak & Flagan, 1989; Filippov, 2000). In these investigations the ratios R_{me}/R_{geo} and R_{me}/R_g approached approximately constant plateaus after initially decreasing with increasing N. For the limiting case $d_f \to 3$ one expects $R_{me}/R_{geo} \to 1$. The KR-theory predicts this ratio to 0.83 for the exact cut-off function and to 0.81 for the Gaussian approximation, reflecting an atypically large deviation from the correct result. Clearly some caution is warranted when using this formalism to treat the dynamics of almost compact particles.

When the mean free pathlength l of the carrier gas molecules approaches the order of magnitude of R_{geo}, Eqs. (9) and (10) will no longer be valid. The correct transition from the continuum regime to the free molecular regime can be assured by introducing a correction factor of the form

$$C(R_{eff}) = 1 + A\frac{l}{R_{eff}} + Q\frac{l}{R_{eff}}\exp\left(-b\frac{R_{eff}}{l}\right) \tag{22}$$

that modifies Eq. (10) to

$$D = \frac{kTC(R_{eff})}{6\pi\eta R_{me,c}}. \tag{23}$$

Here $R_{me,c}$ denotes the continuum regime value of R_{me}. The constants A, Q, and b must be determined empirically. Recent work by Allen and Raabe (1985) and Cheng, Allen, Gallegos, Yeh, and Peterson (1988) suggests $A = 1.142$, $Q = 0.588$, $b = 0.999$ to represent a valid parameterization for solid spheres as well as for small aggregates. Following Dahneke (1973a–c, 1982) the effective agglomerate radius R_{eff} should be chosen in a manner that achieves a consistent prediction of D in the limiting case $l/R_{geo} \to \infty$. Cai and Sorensen (1994) and Wang and Sorensen (1999) have recently shown that the Epstein equation (Friedlander, 1977)

$$D = \frac{3}{8\rho(1 + (\pi/8)\alpha)R_{me}^2}\left(\frac{mkT}{2\pi}\right)^{1/2} \tag{24}$$

($0 \leqslant \alpha \leqslant 1$), originally derived for ideal compact spheres, also holds for agglomerate particles if R_{me} is chosen as

$$R_{me} = R_0 N^x. \tag{25}$$

Performing static and dynamic light scattering experiments and reanalyzing data published in the literature they found $x = 0.43 \pm 0.03$ for $d_f \approx 1.8$, in good agreement with results of computer simulations on agglomerates formed by diffusion limited cluster–cluster aggregation (Chen et al., 1988). The fact that $x < 0.5$ indicates a certain amount of surface shielding even for situations where $d_f < 2$. Xiong, Pratsinis, and Weimer (1992) proposed the following interpolation formula to estimate the accessible surface area S_{acc} of fractal-like structures over the whole range of the surface fractal dimension $2 \leqslant d_s \leqslant 3$:

$$S_{acc} = 4\pi R_0^2 N^{d_s/3} \left[(d_s - 2) \left(\frac{z}{N} \right)^{1-\gamma} - d_s + 3 \right]. \tag{26}$$

For $d_f \leqslant 2$, $d_s = 3$, and Eq. (26) reduces to

$$S_{acc} = 4\pi R_0^2 z^{1-\gamma} N^{\gamma}. \tag{27}$$

With $z = 1$ (in contrast to $z = 2$ as proposed by Xiong et al.) and $\gamma = 2x = 0.86 \pm 0.06$ this becomes equivalent to Eq. (25), identifying R_{me} with the accessible surface equivalent radius R_{acc}, i.e. the property relevant for mass transfer to the particle surface, under free molecular conditions. This idea is supported theoretically (Meakin, Donn, & Mulholland 1989) and experimentally (Rogak, Baltensperger, & Flagan, 1991; Schmidt-Ott, Baltensperger, Gäggeler, & Jost, 1990). In general γ is expected to be a function of d_f and possibly of other structural parameters, also. Unfortunately, this dependence has not been investigated so far. Lacking more precise information, $\gamma = 0.86$ is therefore assumed to hold for all values of d_s in Eq. (26). Considering the approximate nature of Eq. (26) this should not be a serious problem. Furthermore, with decreasing d_s the term $(d_s - 2)(z/N)^{1-\gamma}$ is more and more outweighed by $3 - d_s$. For volume fractals with $2 \leqslant d_f \leqslant 3$, d_s can be estimated to $6/d_f$. However, for surface fractals much larger values of d_s have sometimes been observed (Farin & Avnir, 1989).

In order to satisfy the requirements $R_{me} = R_{me,c}$ under continuum conditions and $R_{me} = (S_{acc}/4\pi)^{0.5} = R_{acc}$ in the free molecular regime simultaneously R_{eff} must be chosen as

$$R_{eff} = \frac{S_{acc}}{4\pi R_{me,c}}. \tag{28}$$

This completes the formalism used in COSIMA to calculate the translational diffusion coefficient D of fractal-like agglomerate particles. Please note that Eq. (23) differs slightly from the usual implementation of the mobility equivalent radius which reads

$$D = \frac{kTC(R_{me})}{6\pi\eta R_{me}}. \tag{29}$$

This implies

$$R_{me} = R_{me,c} \frac{C(R_{me})}{C(R_{eff})}. \tag{30}$$

Eq. (30) facilitates the comparison of modeling results with experimental data like DMA- or SMPS-measurements. Employing impacting devices, however, the aerodynamic radius R_{ae} is required for data analysis. The latter is defined as the radius of a compact spherical reference particle of density ρ_0 (usually latex sphere) achieving the same final settling velocity as the agglomerate (Kasper, 1982)

$$R_{ae}^2 C(R_{ae}) = \frac{\rho R_m^3 C(R_{me})}{\rho_0 R_{me}}. \tag{31}$$

Inserting Eq. (30) for R_{me} finally yields

$$R_{ae}^2 C(R_{ae}) = \frac{\rho R_m^3 C(R_{eff})}{\rho_0 R_{me,c}} \tag{32}$$

which has to be solved numerically for R_{ae}. Please note that for constant particle mass the value of R_{ae} *decreases* with decreasing d_f, opposite to the behavior of R_{geo} and R_{me}. Consequently, geometrically large sized clusters are often characterized by much smaller aerodynamic radii, a point to be kept in mind when designing impaction devices for agglomerate particles.

2.3. Optical properties

The optical properties of fractal aggregates cannot be adequately described by standard Mie theory (Berry & Percival, 1986; Dobbins & Megarides, 1991; Dobbins et al., 1994). However, powerful tools such as T-matrix theory or discrete dipole approximation are now available which accurately predict the absorption and scattering behavior of particles with almost arbitrarily complex shapes (Mishchenko, Hovenier, & Travis, 2000). Unfortunately, these approaches are numerically much too involved to be used in aerosol simulation codes. Furthermore, detailed structure information is required as input which is not available in many cases. To circumvent these problems it proves highly expedient to resort to approximate statistical-mechanical formalisms based on the Fourier transform of the radial pair distribution function $g(r)$, the so-called structure factor $S(q)$. The optics module of the COSIMA program was developed within the framework of the Rayleigh–Debye–Gans (RDG) approximation (Farias, Köylü, & Carvalho, 1996) which implies the neglect of multiple scattering and self interactions within a fractal like cluster. Assuming a Gaussian form for $S(q)$, the specific absorption cross section σ_{abs} and the specific scattering cross section σ_{sca} are then given by (Dobbins et al., 1994)

$$\sigma_{abs} = \frac{6\pi}{\lambda\rho} \operatorname{Im}\left[\frac{n^2-1}{n^2+2} + \frac{x_p}{15}\left(\frac{n^2-1}{n^2+2}\right)^2\left(\frac{n^4+27n^2+38}{2n^2+3}\right)\right] \tag{33}$$

and

$$\sigma_{sca} = \frac{4\pi\langle N^2\rangle x_p^3}{\lambda\rho\langle N\rangle}\left|\frac{n^2-1}{n^2+2}\right| g(\lambda, \langle R_g^2\rangle, d_f) \tag{34}$$

respectively. Following the treatment of Dobbins et al. (1994), the scattering factor $g(\lambda, \langle R_g^{2\rangle}, d_f)$ is written as

$$g(\lambda, \langle R_g^2 \rangle, d_f) = \left[1 + \frac{4k_p^2 \langle R_g^2 \rangle}{3d_f}\right]^{-d_f/2}. \tag{35}$$

Eq. (33) predicts the specific absorption cross section to be independent of cluster size, in good agreement with recent experimental findings (Dobbins et al., 1994; Schnaiter, Horvath, Naumann, Saathoff, & Schurath, 2003). Extensive theoretical investigations by Farias et al. (1996) have shown that the error introduced by the RDG approximation remains below 10% as long as the radius of the primary particles satisfies the Rayleigh limit, i.e. $2\pi R_0/\lambda < 0.3$. Only for clusters consisting of just a few monomers larger deviations have recently been reported (Mulholland & Mountain, 1999). A recently proposed improved expression for $g(\lambda, R_g^2, d_f)$ (Kazakov & Frenklach, 1998) which, compared to Eq. (35), shows a better overall agreement with T-matrix or discrete dipole calculations regarding the specific scattering coefficient has not been considered for implementation into the COSIMA code since it exhibits a singularity at $d_f = 2$. A comprehensive account on the RDG theory as well as on alternative approaches is given in the review article by Sorensen (2001).

3. Program description

The aerosol-physical core of COSIMA is based on the general dynamic equation (GDE) for aerosol behavior discussed in Gelbard and Seinfeld (1979). The GDE is solved using a sectional representation of the particle size distribution (Gelbard, Tambour, & Seinfeld, 1980) with equidistant discretization according to the logarithm of the mass equivalent radius R_m. Thanks to the introduction of the effective radii discussed in Section 2 the numerical solution of the GDE for fractal aerosols proceeds pretty much along the same lines as in the case of compact spherical particles. Therefore the nuclear aerosol behavior code PARDISEKO (Bunz, 1984; Beonio-Brocchieri et al., 1988) could serve as a convenient platform for the development of COSIMA, keeping it comparable in many aspects to the selection of sectional models reviewed by Seigneur et al. (1986) and more recently by Zhang et al. (1999). Specifically, the extensively tested self-governing Euler–Cauchy algorithm used in PARDISEKO to integrate the GDE has been adopted without modification.

Assuming homogeneous mixing in the chamber volume V except for a diffusional boundary layer of thickness δ_D close to the walls the complete set of differential equations governing the time evolution of the aerosol size distribution can be written as

$$\begin{aligned}\frac{\partial n(R_{m,k}, t)}{\partial t} &= S_k(t) - n(R_{m,k}, t)[\alpha_k^D(t) + \alpha_k^S(t) + \alpha_k^L(t)] \\ &\quad - n(R_{m,k}, t) \sum_{i=1}^{N_s} \left(1 - \frac{\delta_{i,k}}{2}\right) K_{ik} n(R_{m,i}, t) \\ &\quad + \sum_{i=1}^{N_s} \sum_{j=i}^{N_s} K_{ij} n(R_{m,i}, t) n(R_{m,j}, t) \beta_{ij}^k \delta_{k,i+j}\end{aligned} \tag{36}$$

with the deposition coefficients for wall diffusion and sedimentation

$$\alpha_i^{\mathrm{D}} = \frac{D(R_{\mathrm{me},i})A_{\mathrm{D}}}{\delta_{\mathrm{D}} V}, \tag{37a}$$

$$\alpha_i^{\mathrm{S}} = \frac{4\pi\rho R_{\mathrm{m},i}^3 g D(R_{\mathrm{me},i})A_{\mathrm{S}}}{3kTV} \tag{37b}$$

the coagulation kernel

$$K_{ij} = K_{ij}^{\mathrm{B}} + K_{ij}^{\mathrm{G}} \tag{38a}$$

the Brownian coagulation kernel

$$K_{ij}^{\mathrm{B}} = \frac{4\pi[D(R_{\mathrm{me},i}) + D(R_{\mathrm{me},j})][R_{\mathrm{geo},i} + R_{\mathrm{geo},j}]}{1 + G_{ij}}, \tag{38b}$$

$$G_{ij} = \frac{4[D(R_{\mathrm{me},i}) + D(R_{\mathrm{me},j})]}{R_{\mathrm{geo},i} + R_{\mathrm{geo},j}} \sqrt{\frac{\pi m_1 m_2}{8kT(m_1 + m_2)}} \tag{38c}$$

and the gravitational coagulation kernel

$$K_{ij}^{\mathrm{G}} = \varepsilon_{ij}\pi(R_{\mathrm{geo},i} + R_{\mathrm{geo},j})^2 \frac{g|m_i D(R_{\mathrm{me},i}) - m_j D(R_{\mathrm{me},j})|}{kT}, \tag{38d}$$

$$\varepsilon_{ij} = \frac{\kappa}{2} \frac{R_{\mathrm{geo},i}^2}{(R_{\mathrm{geo},i} + R_{\mathrm{geo},j})^2} + 1 - \kappa, \quad 0 \leqslant \kappa \leqslant 1, R_{\mathrm{geo},i} < R_{\mathrm{geo},j}. \tag{38e}$$

The source rate $S_k(t)$ and the leakage function $\alpha_k^{\mathrm{L}}(t)$ have to be provided as input. When analyzing results of aerosol chamber experiments $\alpha_k^{\mathrm{L}}(t)$ may be used to simulate sampling losses. The interpolation factor

$$\beta_{ij}^k = \frac{m_{k\pm1} - (m_i + m_j)}{m_{k\pm1} - m_k}, \quad \begin{array}{l} + \text{ for } (m_i + m_j) \in (m_k, m_{k+1}), \\ - \text{ for } (m_i + m_j) \in (m_{k-1}, m_k) \end{array} \tag{39}$$

in Eq. (36) accounts for the fact that the chosen size discretization is not equidistant in mass. Following Fuchs (1964) and Okuyama, Kousaka, Yamamoto, and Hosokawa (1986) the size dependence of the diffusive boundary layer thickness δ_{D} is expressed as

$$\delta_{\mathrm{D}} = k_{\mathrm{D}} \left(\frac{D}{D_0}\right)^a. \tag{40}$$

Adopting the parameterization $k_{\mathrm{D}} = 0.005$ m, $a = 0.274$ (Bunz & Dlugi, 1991) results in good agreement between measured and calculated deposition losses for compact as well as for fractal-like particles.

Eq. (38b) interpolates the Brownian coagulation kernel between the limiting cases of continuum and free molecular flow. For purely Brownian diffusion it assumes a Smoluchowsky mean-field form similar to the one validated by Ziff, McGrady, and Meakin (1985). Applying Eqs. (5) and (21) to

Eq. (38b), one obtains in the limit $l/R_{\mathrm{eff}} \to 0$:

$$K_{ij}^{\mathrm{B}}(\mathrm{cont}) = \frac{2kT}{3\eta h_{\mathrm{KR}}}\left(\frac{1}{N_i^{1/d_{\mathrm{f}}}} + \frac{1}{N_j^{1/d_{\mathrm{f}}}}\right)\left(N_i^{1/d_{\mathrm{f}}} + N_j^{1/d_{\mathrm{f}}}\right). \tag{41a}$$

Under free molecular conditions the expression proposed by Matsoukas and Friedlander (1991) is recovered augmented by an additional factor $f^{2/d_{\mathrm{f}}}$:

$$K_{ij}^{\mathrm{B}}(\mathrm{free}) = \sqrt{\frac{6kTR_0}{\rho}\left(\frac{1}{N_i} + \frac{1}{N_j}\right)}\, f^{2/d_{\mathrm{f}}}(N_i^{1/d_{\mathrm{f}}} + N_j^{1/d_{\mathrm{f}}})^2. \tag{41b}$$

Please note that for compact spherical particles ($d_{\mathrm{f}} = 3$, $f = 1$) $R_{\mathrm{me}} = R_{\mathrm{geo}}$, and Eq. (38b) reduces to the well-known harmonic mean coagulation kernel as considered by Pratsinis (1988) and more recently by Park, Lee, Otto, and Fissan (1999).

Considering gravitational coagulation a straightforward extension of the formalism developed by Pruppacher and Klett (1997) to the case of fractal particles leads to the following expression for the collision efficiency:

$$\varepsilon_{ij} = \frac{1}{2}\frac{R_{\mathrm{geo},i}^2}{(R_{\mathrm{geo},i} + R_{\mathrm{geo},j})^2}, \quad R_{\mathrm{geo},i} < R_{\mathrm{geo},j}. \tag{42}$$

The factor ε_{ij} accounts for the fact that small particles may follow the flow around lager ones, resulting in significantly reduced coagulation rates compared to purely geometrically controlled interception ($\varepsilon_{ij} = 1$). However, Eq. (42) is only applicable if penetration of the particles by the carrier gas may be neglected. For agglomerates characterized by low fractal dimensions this is not the case. Eq. (42) then defines a lower limit for the coagulation frequency, while the upper limit is obtained with $\varepsilon_{ij} = 1$. Good agreement between theory and recent experimental results could be obtained by employing the simple interpolation ansatz Eq. (38e) between lower and upper limit (Möhler, Naumann, & Schöck, 1994; Möhler & Naumann, to be published). For acetylene soot κ was determined to 0.86 indicating that gravitation induced capturing of small particles by larger ones is much more effective for fractal agglomerates than for compact species.

4. Code validation

4.1. Comparison of COSIMA predictions with theoretical and simulation results on the asymptotic behavior of fractal aerosols

Vermury and Pratsinis (1995) have extended the code of Landgrebe and Pratsinis (1990), which is claimed to be very accurate by the authors, to treat the dynamics of fractal agglomerates in the limits of continuum and free molecular conditions. Since they did not consider the effect of hydrodynamic interactions between the primary particles, the continuum regime coagulation kernel used in their study (Eq. (6) of Vermury & Pratsinis (1995)) differs from the one implemented in COSIMA, Eq. (41a), by the inverse Kirkwood–Riseman factor $1/h_{\mathrm{KR}}$. Inspecting Eq. (21) one easily recognizes that for volume fractal dimensions d_{f} well below 3 the term $1/h_{\mathrm{KR}}$ assumes values

much larger than 1, e.g. 1.92 and 2.25 for $d_f = 2.0$ and 1.8, respectively, resulting in significantly enhanced coagulation rates. Considering the free molecular regime, the coagulation kernel employed by Vermury and Pratsinis (1995) is identical to the one proposed by Matsoukas and Friedlander (1991), which differs from the expression used in COSIMA (Eq. (41b)) by a factor f^{2/d_f}. With $f = 1.43$ (Naumann & Bunz, 1991; Nyeki & Colbeck, 1994) this also leads to increased coagulation rates, although the effect is smaller than in the continuum limit. Please note that for agglomerates consisting of non-overlapping monomers the lower limit for the volume filling factor is $f = 1.35$. Therefore, the choice $f = 1$ bringing Eq. (41b) into coincidence with the expression of Matsoukas and Friedlander (1991) cannot be justified for physical reasons. Due to the differences outlined above the simulated time evolutions of the number concentrations of fractal aerosols reported by Vermury and Pratsinis (1995) are not directly comparable to the respective COSIMA predictions. This does not apply, however, to the forms of the dimensionless self preserving size distributions attained in the long time regime and their dependence on d_f. Since h_{KR} and f^{2/d_f} are independent of particle size, all coagulation rates are enhanced by the same factor provided the aerosol is characterized by one constant fractal dimension. Therefore the shape of the self preserving size distributions will not be affected by h_{KR} or by f^{2/d_f}, in contrast to the time needed to establish them. Vermury, Kusters, and Pratsinis (1994) have shown that already in the case of compact spherical particles the form of calculated self-preserving size distributions is very sensitive to the numerical stability of sectional codes. The treatment of fractal aerosols represents an even more demanding task due to the enhanced coagulation rates encountered in these systems. In the following, dimensionless self preserving size distributions computed by COSIMA for various values of d_f under continuum and free molecular limiting conditions are compared to the results documented in Vermury and Pratsinis (1995).

All scenarios are started with an initial particle concentration of $1 \times 10^{22}/m^3$. The pressure is 1.013×10^5 Pa and the material density is 4200 kg/m^3. In the continuum regime, the initial particle size is $R_0 = 0.25$ μm, and the temperature is $T = 300\,K$. For the free molecular cases the initial particle size is $R_0 = 0.5$ nm, and the temperature is $T = 1800\,K$. The range of volume fractal dimensions covered in the free molecular regime is $d_f = 2.0$–3.0, while under continuum conditions the range $d_f = 1.8$–3.0 is considered. The case $d_f = 1.0$, which has also been treated by Vermury and Pratsinis (1995), is omitted here for reasons discussed at the beginning of Section 2. The results are presented in Figs. 1 and 2, where the self preserving dimensionless particle density function $\Psi(v_k,t) = c_v n(v_k,t)/c_n^2$ is plotted versus the dimensionless particle volume $\eta_k = c_n v_k/c_v$ for continuum and free molecular conditions, respectively, and in Fig. 3, which shows the standard deviation σ of the size distribution as a function of d_f. There is perfect agreement between the predictions of both codes. This is specifically interesting in view of the fact that Vermury and Pratsinis (1995) noted a significant discrepancy for the dependence of σ on d_f in the free molecular regime with the results obtained by Wu and Friedlander (1993b) using a Monte Carlo technique. Thus it appears that the data reported by Wu and Friedlander (1993a) might be in error. Tandon and Rosner (1999) also employed a Monte Carlo scheme to evaluate self preserving size distributions in the continuum regime based on the same coagulation kernel as used by Vermury and Pratsinis (1995). Within the numerical scatter of their data there is good agreement with the predictions of the sectional codes. The aerosol physical implications of the simulation results presented in Figs. 1–3 have been discussed in detail in Vermury and Pratsinis (1995) and will, therefore, not be repeated here. Please note, however, that the self preserving size distributions deviate significantly from a log-normal shape, especially in the free molecular regime. In the continuum regime $\sigma = 1.320$ would be expected independent of d_f

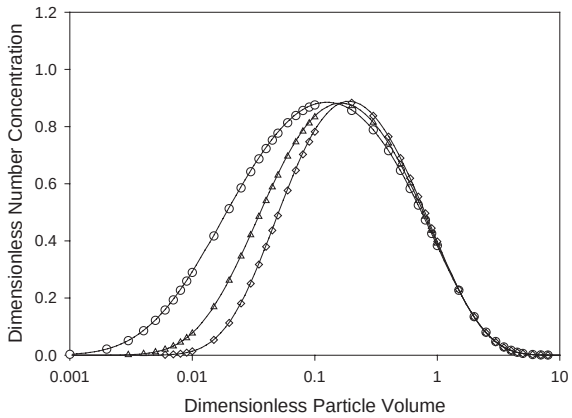

Fig. 1. Continuum regime self preserving size distributions as a function of d_f as predicted by the Vermury and Pratsinis code (symbols) and by COSIMA (lines): $d_f = 3.0$ (circles), $d_f = 2.2$ (triangles), $d_f = 1.8$ (diamonds).

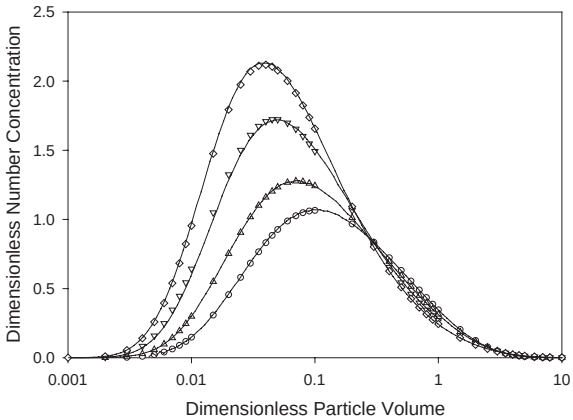

Fig. 2. Free molecular regime self preserving size distributions as a function of d_f as predicted by the Vermury and Pratsinis code (symbols) and by COSIMA (lines): $d_f = 3.0$ (circles), $d_f = 2.6$ (upward triangles), $d_f = 2.2$ (downward triangles) $d_f = 2.0$ (diamonds).

for strictly log-normal behavior (Jain & Kodas, 1998) in clear contradiction to the trend displayed by Fig. 3. Under free molecular conditions the asymptotic value of σ should rise from 1.355 for $d_f = 3.0$ to 1.48 for $d_f = 2.0$ if the log-normal assumption were fulfilled (Jain & Kodas, 1998). In fact, a much larger increase is predicted by the sectional models (see Fig. 3). Therefore, the analytical solutions to the Brownian coagulation equations for fractal aerosols published by Park, Xiang, and Lee (2000) and by Park and Lee (2002) which assume log-normal size distributions are of limited use for the validation of sectional codes.

Wu and Friedlander (1993b) have shown theoretically, that under free molecular conditions the asymptotic slope of $\ln[c_n(t)/c_n(t=0)]$ versus $\ln(t)$ is given by $2d_f/(4-3d_f)$. This result is not affected by the additional factor f^{2/d_f} by which the coagulation kernel implemented in COSIMA

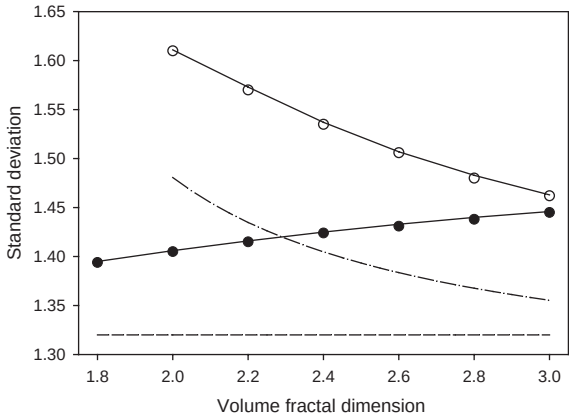

Fig. 3. Standard deviation of self preserving size distributions as a function of d_f under continuum (full symbols) and free molecular (open symbols) conditions as predicted by the Vermury and Pratsinis code (symbols) and by COSIMA (—). For comparison, analytical results assuming a strictly log-normal behavior are also included for continuum (- - -) and free molecular (-.-) conditions.

Table 1
Dependence of the asymptotic slope of $\ln[c_n(t)/c_n(t=0)]$ vs. $\ln(t)$ on the volume fractal dimension d_f under free molecular conditions

d_f	Theory (Wu & Friedlander, 1993b)	COSIMA
2.0	−2.000	−1.993
2.2	−1.692	−1.690
2.4	−1.500	−1.498
2.6	−1.368	−1.364
2.8	−1.273	−1.271
3.0	−1.200	−1.199

differs from the one used by Wu and Friedlander (1993b), although the asymptotic regime is reached faster if this factor is accounted for. In Table 1 theoretically predicted asymptotic slopes are compared to the results of COSIMA simulations based on the scenarios of Vermury and Pratsinis (1995) outlined above. There is very good agreement between theory and computer model predictions.

4.2. Comparison of COSIMA predictions with experimental results

In this section COSIMA simulation results will be compared to new experimental findings on the dynamics of Diesel and graphite spark generated soot aerosols obtained during the AIDA soot characterization campaign (1999). Here, the presentation will mainly focus on code parameterization and performance, while the COSIMA assisted analysis and aerosol physical interpretation of the experimental findings are exemplified in more detail in the companion papers by Wentzel et al. (2003), Schnaiter et al. (2003), Saathoff et al. (2003b), and Saathoff et al. (2003c). Brief accounts

on the performance of COSIMA may also be found in Möhler et al. (1994) for acetylene soot and in Naumann and Bunz (1992) for uranium dioxide aerosol. Please note, however, that in these older studies a simple step cutoff function was used for $h(r)$ instead of the much more elaborated expression Eq. (19). Furthermore, the effective radius R_{eff} required for the slip correction in the transition regime was determined differently from Eq. (28).

The measurements referred to (experiments #2 and #3 as listed in Saathoff (2003)) were conducted under ambient conditions ($T = 296$ K, $p \approx 1.0 \times 10^5$ Pa) in the AIDA facility of the Research Center Karlsruhe ($V = 84.3$ m^3, $A_{\mathrm{D}} = 103$ m^2, $A_{\mathrm{S}} = 12.6$ m^2). Its technical and analytical equipment is described in Saathoff (2003). Diesel soot aerosol was obtained from a Volkswagen 4-cylinder turbo engine while graphite spark soot was produced using two commercial generators (GFG 1000, Palas) similar to the one described in Helsper et al. (1993). The experimental details are discussed in the companion papers cited above.

Extensive parameter studies have shown that dynamical processes in agglomerate aerosols such as diffusion, sedimentation and coagulation are highly sensitive to small variations of d_{f}. A less pronounced but still significant dependence is also observed for the primary particle radius R_0. Therefore, the intercomparison of measured and simulated time evolutions of mass and number concentrations as well as mobility based size distributions provides a reliable route towards determining d_{f} and R_0 simultaneously (Kamm et al., 1999; Wentzel et al., 2003) which does not require the laborious and somewhat problematic analysis of TEM images. With mass concentration and mobility size distribution both available for a given time t, d_{f} and R_0 cannot be varied independently. This is seen by combining Eqs. (4), (21) and (30), thereby establishing a relation between the mass equivalent radius R_{m} and the mobility equivalent radius R_{me},

$$\left(\frac{R_{\mathrm{m}}}{R_0}\right)^3 = N = \frac{1}{f}\left(\frac{R_{\mathrm{me}}}{h_{\mathrm{KR}}R_0}\,\frac{C(R_{\mathrm{eff}})}{C(R_{\mathrm{me}})}\right)^{d_{\mathrm{f}}} \tag{43}$$

which has to be solved iteratively in general, as R_{eff} depends on the particle mass. Eq. (43) allows to convert a measured mobility size distribution into the corresponding mass distribution. Integrating over all size classes yields an estimate for the mass concentration which can be compared to the experimentally determined value. For a given material density ρ and with f already fixed to 1.43, d_{f} and R_0 are thus uniquely linked, leaving only one independent parameter. In the cases under consideration the relative humidity did not exceed 47%. Therefore, agglomerate restructuring due to capillary condensation can be neglected and d_{f} is assumed to be independent of time. All simulations discussed below were initialized with size distributions measured immediately after homogeneous mixing had been established in the AIDA chamber. Subsequently d_{f} and R_0 were varied for optimum agreement between experimental and numerical results. The parameters providing the best overall fit to the measured data are summarized in Table 2.

Fig. 4a shows measured and calculated time evolutions of mass and number concentration for Diesel soot. The time $t = 0$ refers to the end of aerosol feeding. Because the light-extinction of fractal-like soot particles in the UV-VIS region is proportional to their mass concentration to a very good approximation (Dobbins et al., 1994; Schnaiter et al., 2003), this information is included in Fig. 4a to complement the filter samples which could only be taken at the beginning and at the end of the experiments. Conserving the initial mobility size distribution while varying d_{f} produces a dramatic dependence of the modeled mass concentration profiles on this parameter.

Table 2
Optimum parameters obtained by comparing simulated and observed results for Diesel and graphite spark soot aerosols

	Diesel soot	Graphite spark soot
d_f	2.0 ± 0.1	2.0 ± 0.1
R_0 (nm)	13.5 ± 1.5	3.7 ± 0.4
f[a]	1.43	1.43
ρ (kg/m^3)[a]	1700	2000
n (473 nm)[b]	1.43 + 0.64i	2.29 + 1.00i

[a]Not varied.
[b]Interpolated from experimental results of Schnaiter et al. (2003) for 450 and 550 nm.

Only a narrow range of fractal dimensions around $d_f = 2.0$ is compatible with the measured values. The same applies to the light extinction at $\lambda = 473$ nm calculated by summing the contributions from Eqs. (33) and (34). On the scale of Fig. 4a the resulting graphs are indistinguishable from the corresponding time evolutions of the mass concentration although the scattering term, which depends on particle size, contributes about 20% to the total extinction. The development of the calculated number concentration exhibits a less pronounced but still significant dependence on d_f, especially for longer times, reflecting the increase of coagulation rates with decreasing volume fractal dimension. Fig. 4b compares mobility size distributions simulated for different values of d_f with the respective measured ones. The model runs were initialized at $t = 3$ min. After 5 h the effect of d_f on the modeled time evolutions becomes clearly visible. After 27 h again only a narrow range of d_f values remains compatible with the experimental results. Choosing $d_f = 2.0$ and $R_0 = 13.5$ nm results in good overall agreement between measured and simulated data. The error limits given in Table 2 reflect the parameter range associated with the uncertainties of the measurements. The primary particle radius $R_0 = 13.5 \pm 1.5$ nm is consistent with $R_0 = 11.3 \pm 3$ nm obtained by Wentzel et al. (2003) by analyzing TEM images.

Fig. 5a visualizes the calculated and observed time evolutions of mass and number concentration and of light extinction at $\lambda = 473$ nm for graphite spark generated soot. Qualitatively this aerosol behaves very similar to Diesel soot. Quantitatively, however, one observes a much sharper decrease of c_n with time, since the graphite spark soot experiment was started with a somewhat higher mass and an order of magnitude higher number concentration. Furthermore, the primary particles of graphite spark soot are much smaller than those of Diesel soot. As both aerosols are characterized by similar fractal dimensions this results in larger collisional cross sections for a given particle mass and hence in higher coagulation rates in the case of graphite spark soot. This effect is clearly demonstrated in Fig. 5b where simulated and measured time evolutions of the mobility size distribution are shown. At $t = 67$ min, only 52 min after the start of the simulation, the range of fractal dimensions compatible with experiment has already narrowed to $d_f = 2.0 \pm 0.1$. At $t = 213$ min the considered 10% variation around the optimum value $d_f = 2$ causes very large discrepancies compared to the observed behavior. Theoretically, the enhanced coagulation rates of graphite spark soot compared to Diesel soot are expected to manifest themselves also in the optical aerosol properties. The mass concentration is predicted to decay slightly faster than the light extinction during the early stages of the experiment since the simulated specific

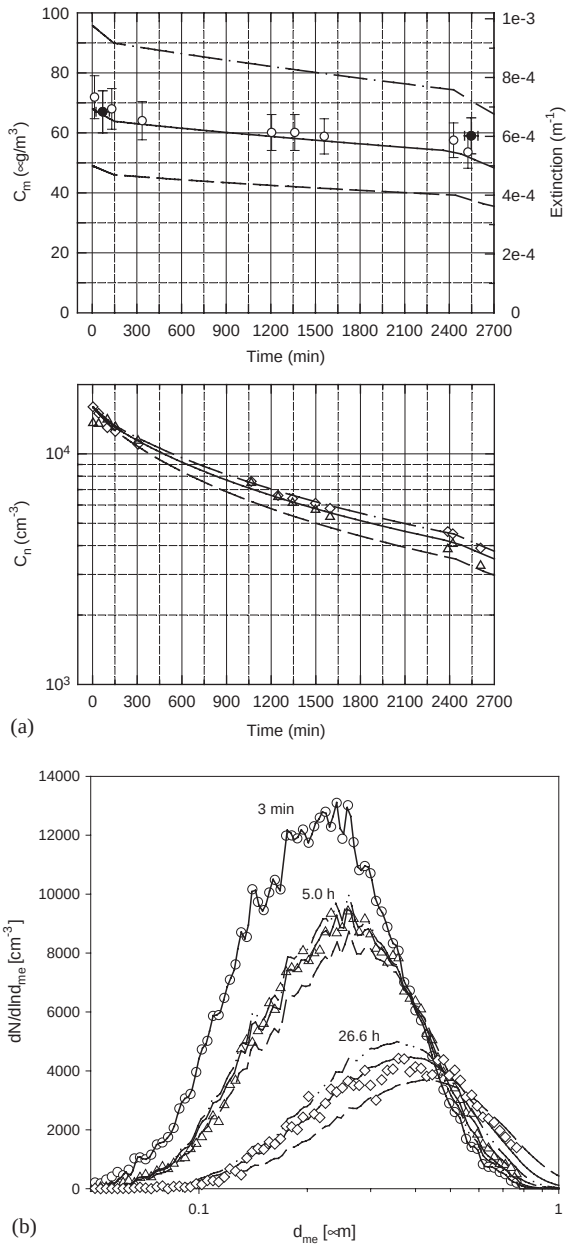

Fig. 4. (a) Experimental and simulated time evolutions of mass and number concentration and of light extinction at 473 nm for Diesel soot aerosol. Experiment: Mass concentration (full circles), extinction (open circles), CNC (diamonds), SMPS (triangles). Simulation: ---, $d_f = 1.8$, —, $d_f = 2.0$, -.-, $d_f = 2.2$. The steps at the beginning and at the end of the experiment are due to sampling losses. (b) Experimental and simulated time evolution of the mobility based size distribution for Diesel soot: experiment (symbols). Simulation: ---, $d_f = 1.8$, —, $d_f = 2.0$, -..-, $d_f = 2.2$.

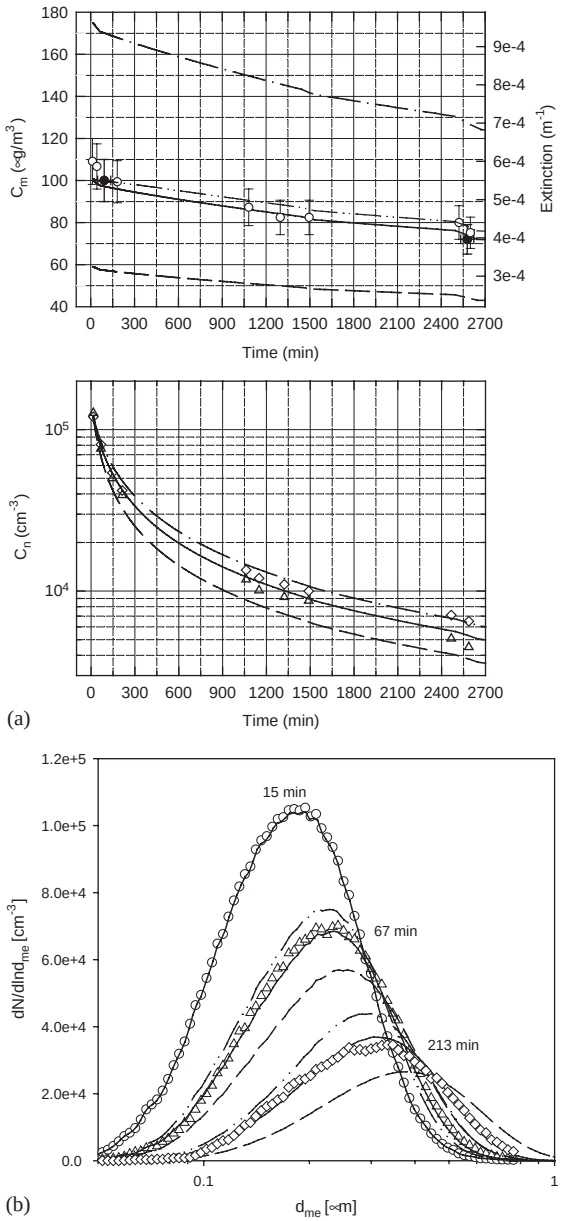

Fig. 5. (a) Same as Fig. 4a for graphite spark soot, supplemented by extinction predicted for $d_f = 2.0$ (-..-). (b) Same as Fig. 4b for graphite spark soot.

scattering cross section increases significantly as a result of rapid particle growth. Unfortunately, the measurements presented in Fig. 5a are not accurate enough to verify this model prediction unambiguously. However, for fractal aerosols undergoing very rapid coagulation the assumption of proportionality between light extinction and mass concentration might be less accurate as in the

cases considered above. The closest overall fit of simulated on observed data for graphite spark soot is achieved with $d_f = 2.0$ and $R_0 = 3.7$ nm, consistent with the values $d_f = 2.1$ measured by Weingartner, Baltensperger, and Burtscher (1995) combining mobility sizing with low pressure impaction, and $R_0 = 3.3 \pm 0.9$ nm obtained by Wentzel et al. (2003) from the analysis of TEM images.

For both Diesel and graphite spark soot the average mobility equivalent diameter was around 200 nm during the early stages of the experiment and above 500 nm after 40 h. Comparing these values to the mean free pathlength of the carrier gas of about 70 nm, it becomes obvious that the experiments were started well within the transition regime passing over to almost continuum conditions during the later stages. Thus, the good agreement between simulated and observed data lends credit to the approximate transition regime interpolation scheme established by Eqs. (22) and (28). In passing from transition regime to continuum conditions the effect of hydrodynamic interactions and screening on the dynamics of agglomerate aerosols is expected to become more and more important. Therefore, in Figs. 6a and b the experimentally determined time evolutions of the mobility size distribution for graphite spark soot and Diesel soot are compared with simulations including and excluding the Kirkwood–Riseman correction term h_{KR}. Since $h_{KR} < 1$ for volume fractal dimensions well below 3, neglecting this term in Eq. (43) (i.e. assuming $h_{KR} = 1$) relates a smaller particle mass to a given mobility radius R_{me}. In order to match the mass concentration determined from the mobility size distribution to the directly measured one d_f has to be increased from 2.0 to 2.37 in the case of graphite spark soot, accordingly. This value differs considerably from the experimental result of Weingartner, Baltensperger, and Burtscher (1995). Furthermore, Fig. 6a clearly reveals that the simulation initialized with $d_f = 2.37$, $R_0 = 3.7$ nm, and $h_{KR} = 1$ poorly reproduces the experimental observations. A similar pattern emerges for Diesel soot (Fig. 6b), although the diffusion, coagulation, and sedimentation rates of both aerosols differ significantly as outlined above. Retaining the monomer radius of Diesel soot at $R_0 = 13.5$ nm while neglecting the Kirkwood–Riseman term requires d_f to be increased from 2.0 to 2.51 in order to restore consistency between the mass concentration calculated from the initial mobility size distribution and the measured one. However, as in the case of graphite spark soot the simulation initialized with $h_{KR} = 1$ badly fails to reproduce the experimentally observed time evolution of the mobility size distribution. Another possibility to assure consistency between mobility sizing and mass concentration would be to significantly increase R_0 on the cost of d_f. This measure, however, does not improve the simulation results and is inconsistent with the TEM results of Wentzel et al. (2003). On the other hand the simulations based on the parameters given in Table 2 and including the Kirkwood–Riseman correction nicely reproduce all available experimental data. Evidently hydrodynamic interactions and screening must be accounted for when modeling the continuum or transition regime dynamics of fractal like aerosols.

With initial mass concentrations as low as 67 $\mu g/m^3$ in the case of Diesel soot and 100 $\mu g/m^3$ for graphite spark soot one already observes a strong effect of the volume fractal dimension on the coagulation dynamics of ramified agglomerate particles. If significantly higher mass concentrations are to be considered, e.g. in technical processes or in nuclear accident scenarios, the influence of d_f on the particle growth rates becomes even more pronounced (Naumann & Bunz, 1992). It has been shown that under such extreme circumstances gravitational coagulation starts to dominate the growth of fractal-like particles (Naumann & Bunz, 1992; Möhler et al., 1994; Möhler and Naumann, to be published).

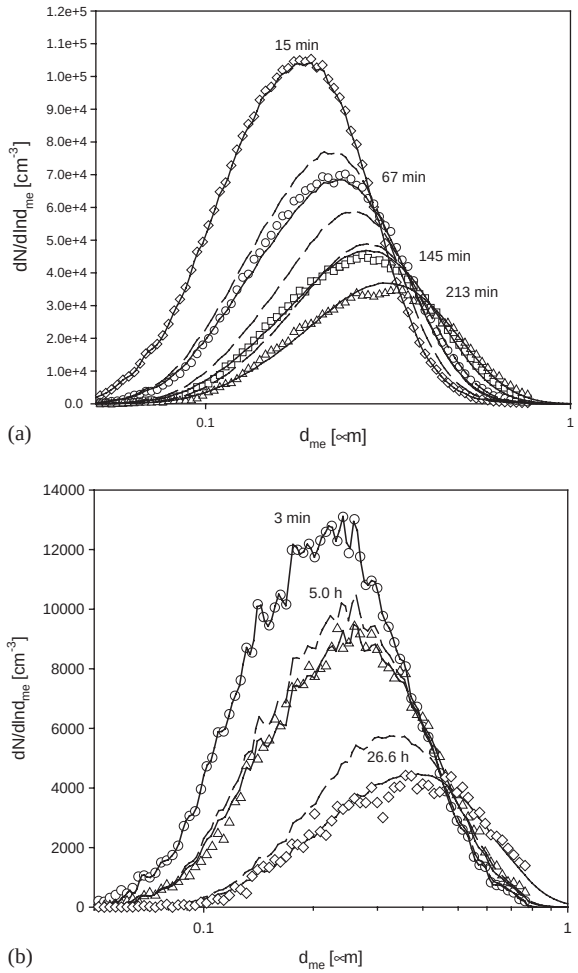

Fig. 6. (a) Effect of the exclusion of hydrodynamic interactions and screening on the simulated time evolution of the mobility based size distribution for graphite spark soot: experiment (symbols), simulation including the Kirkwood–Riseman term (- - -), simulation neglecting the Kirkwood–Riseman term (—). (b) Same as Fig. 6a for Diesel soot.

5. Conclusion

The computer model COSIMA presented in this paper has been developed from first principle aerosol mechanics and optics. The sectional representation of the size distribution greatly facilitates the usage of experimentally determined input data. The apparent structural irregularity of agglomerates is accounted for by defining a set of effective radii using fractal scaling laws. From this formalism the fractal pre-factor k_g is predicted in good agreement with recent computer simulation results on DLCCA clusters. Regarding particle mobility, hydrodynamic interactions and screening are considered within the framework of the Kirkwood–Riseman theory. Compared to the dynamics of compact spheres largely enhanced coagulation and growth rates accompanied by diminished depositional loss are thus predicted for agglomerates of low volume fractal dimensionality. Finally,

light scattering and absorption by fractal particles are modeled based on the Rayleigh–Debye–Gans theory. The code has been verified by comparing its predictions against theoretical and simulation results documented in the literature as well as new experimental data on the dynamics and optical properties of Diesel and graphite spark soot. In this context evidence is presented that hydrodynamic interactions and screening must be accounted for in order to interpret the measured data consistently. The Kirkwood–Riseman correction significantly enhances the mobility of agglomerate particles characterized by low volume fractal dimensions but does not affect the form of the self preserving distributions attained in the long time regime.

By now the model is restricted to the simulation of aerosols with monodisperse primary particles and constant volume and surface fractal dimensions. In order to study particle restructuring processes, e.g. as a result of water uptake in humid environments or due to coating by low-volatile organic substances, time dependent fractal dimensions or even distributions of fractal dimensions would be required. The same holds true if mixtures of particles characterized by different fractal dimensions are considered. More generalized approaches have recently been considered e.g. by Bushell and Amal (1998), Tandon and Rosner (1999), and by Kostoglou and Konstandopoulos (2001). The ongoing theoretical and modeling efforts towards extending the COSIMA code are significantly benefiting from the experimental results obtained during the AIDA soot characterization campaign 1999.

Acknowledgements

The author would like to thank Helmut Bunz for providing him with the source of his aerosol code PARDISEKO IV. Harald Saathoff, Martin Schnaiter, and Ottmar Möhler are acknowledged for valuable discussions facilitating the use of their experimental data in the COSIMA validation process.

References

Allen, M. D., & Raabe, O. G. (1985). Slip correction measurements of spherical solid aerosol particles in an improved Millikan apparatus. *Aerosol Science and Technology*, *4*, 269–286.

Avnir, D. (Ed.) (1989). *The fractal approach to heterogeneous chemistry*. Chichester: Wiley.

Beonio-Brocchieri, F., Bunz, H., Schöck, W., Dunbar, I. H., Gauvain, J., Miyahara, S., Himeno, Y., Soda, K., & Yamano, N. (1988). Nuclear aerosol codes. *Nuclear Technology*, *81*, 193–204.

Berry, M. V., & Percival, I. C. (1986). Optics of fractal clusters such as smoke. *Optica Acta*, *33*, 577–591.

Bohren, C. F., & Huffman, D. R. (1998). *Absorption and scattering of light by small particles*. New York: Wiley.

Botet, R., & Jullien, R. (1986). Intrinsic anisotropy of clusters in cluster–cluster aggregation. *Journal of Physics A*, *19*, L907–L912.

Botet, R., Rannou, P., & Cabane, M. (1995). Sensitivity of some optical properties of fractals to the cut-off functions. *Journal of Physics A*, *28*, 297–316.

Brasil, A. M., Farias, T. L., & Carvalho, M. G. (2000). Evaluation of the fractal properties of cluster–cluster aggregates. *Aerosol Science and Technology*, *33*, 440–454.

Bunz, H. (1984). *PARDISEKO IV—a computer code for calculating the aerosol behavior in closed vessels*. Report KfK 3545 e.

Bunz, H., & Dlugi, R. (1991). Numerical studies on the behaviour of aerosols in smog chambers. *Journal of Aerosol Science*, *22*, 441–465.

Bushell, G., & Amal, R. (1998). Fractal aggregates of polydisperse particles. *Journal of Colloid and Interface Science*, *205*, 459–469.

Cai, J., Lu, N. L., & Sorensen, C. M. (1995). Analysis of fractal cluster morphology parameters: Structural coefficient and density autocorrelation function cutoff. *Journal of Colloid and Interface Science*, *171*, 470–473.

Cai, J., & Sorensen, C. M. (1994). Diffusion of fractal aggregates in the free molecular regime. *Physical Review E*, *50*, 3397–3400.

Chen, Z.-Y., Weakliem, P. C., & Meakin, P. (1988). Hydrodynamic radii of diffusion-limited aggregates and bond-percolation clusters. *Journal of Chemical Physics*, *89*, 5887–5889.

Cheng, Y.-S., Allen, M. D., Gallegos, D. P., Yeh, H.-C., & Peterson, K. (1988). Drag force and slip correction of aggregate aerosols. *Aerosol Science and Technology*, *8*, 199–214.

Colbeck, I., & Wu, Z. (1994). Measurement of the fractal dimensions of smoke aggregates. *Journal of Physics D*, *27*, 670–675.

Dahneke, B. E. (1973a). Slip correction factors for nonspherical bodies—I. Introduction and continuum flow. *Aerosol Science*, *4*, 139–145.

Dahneke, B. E. (1973b). Slip correction factors for nonspherical bodies—II. Free molecule flow. *Aerosol Science*, *4*, 147–161.

Dahneke, B. E. (1973c). Slip correction factors for nonspherical bodies—III. The form of the general law. *Aerosol Science*, *4*, 163–170.

Dahneke, B. E. (1982). Viscous resistance of straight-chain aggregates of uniform spheres. *Aerosol Science and Technology*, *1*, 179–185.

Dobbins, R. A., & Megarides, C. (1991). Absorption and scattering of light by polydisperse aggregates. *Applied Optics*, *30*, 4747–4754.

Dobbins, R. A., Mulholland, G. W., & Bryner, N. P. (1994). Comparison of a fractal smoke optics model with light extinction measurements. *Atmospheric Environment*, *28*, 889–897.

Doi, M., & Edwards, S. F. (1986). *The theory of polymer dynamics*. Oxford: Clarendon Press.

Farias, T. L., Köylü, Ü. O., & Carvalho, M. G. (1996). Range of validity of the Rayleigh–Debye–Gans theory for optics of fractal aggregates. *Applied Optics*, *35*, 6560–6567.

Farin, D., & Avnir, D. (1989). The fractal nature of molecule–surface interactions and reactions. In D. Avnir (Ed.), *The fractal approach to heterogeneous chemistry* (pp. 271–293). Chichester: Wiley.

Filippov, A. V. (2000). Drag and torque on clusters of N arbitrary spheres at low Reynolds number. *Journal of Colloid and Interface Science*, *229*, 184–195.

Friedlander, S. K. (1977). *Smoke, dust, and haze*. New York: Wiley.

Fuchs, N. A. (1964). *The mechanics of aerosols*. Oxford: Pergamon Press.

Gelbard, F., & Seinfeld, J. (1979). The general dynamic equation for aerosols—theory and application to aerosol formation and growth. *Journal of Colloid and Interface Science*, *68*, 363–382.

Gelbard, F., Tambour, Y., & Seinfeld, J. (1980). Sectional representations for simulating aerosol dynamics. *Journal of Colloid and Interface Science*, *76*, 541–556.

Happel, J., & Brenner, H. (1963). *Low Reynolds number hydrodynamics with special applications to particulate media*. Boston: Nijhoff.

Helsper, C., Mölter, W., Löffler, F., Wadenpohl, C., Kaufmann, S., & Wenninger, G. (1993). Investigation of a new aerosol generator for the production of carbon aggregate particles. *Atmospheric Environment*, *27A*, 1271–1275.

Jain, S., & Kodas, T. T. (1998). Asymptotic widths of size distributions resulting from collisional growth assuming log-normally distributed fractal aggregates. *Journal of Aerosol Science*, *29*, 259–261.

Kamm, S., Möhler, O., Naumann, K.-H., Saathoff, H., & Schurath, U. (1999). The heterogeneous reaction of ozone with soot aerosol. *Atmospheric Environment*, *33*, 4651–4661.

Kasper, G. (1982). Dynamics and measurement of smokes. I. Size characterization of nonspherical particles. *Aerosol Science and Technology*, *1*, 187–199.

Kazakov, A., & Frenklach, M. (1998). Dynamic modeling of soot particle coagulation and aggregation: Implementation with the method of moments and application to high-pressure laminar premixed flames. *Combustion and Flame*, *114*, 484–501.

Kirkwood, J. G., & Riseman, J. (1948). The intrinsic viscosities and diffusion constants of flexible macromolecules in solution. *Journal of Chemical Physics*, *16*, 565–573.

Kolb, M. (1985). Effects of the growth mechanism on the structure of aggregation clusters. *Journal de Physique Lettres*, *46*, L–631–L-637.

Kostoglou, M., & Konstandopoulos, A. G. (2001). Evolution of aggregate size and fractal dimension during Brownian coagulation. *Journal of Aerosol Science*, *32*, 1399–1420.

Landgrebe, J. D., & Pratsinis, S. E. (1990). A discrete sectional model for powder production by gas phase chemical reaction and aerosol coagulation in the free molecular regime. *Journal of Colloid and Interface Science*, *139*, 63–86.

Mandelbrodt, B. (1982). *The fractal geometry of nature*. San Francisco: Freeman.

Matsoukas, T., & Friedlander, S. K. (1991). Dynamics of aerosol agglomerate formation. *Journal of Colloid and Interface Science*, *146*, 495–506.

Meakin, P. (1998). *Fractals, scaling and growth far from equilibrium*. Cambridge: Cambridge University Press.

Meakin, P., Donn, B., & Mulholland, G. W. (1989). Collisions between point masses and fractal aggregates. *Langmuir*, *5*, 510–518.

Meakin, P., & Vicsek, T. (1985). Internal structure of diffusion limited aggregates. *Physical Review A*, *32*, 685–688.

Mishchenko, M., Hovenier, J. W., & Travis, L. D. (Eds.) (2000). *Light scattering by nonspherical particles*: *Theory*, *measurements*, *and applications*. San Diego, Academic Press.

Möhler, O., Naumann, K.-H., & Schöck, W. (1994). Dynamic behaviour of fractal soot aerosols. *Journal of Aerosol Science*, *25*, S303–S304.

Mountain, R. D., & Mulholland, G. W. (1988). Light scattering from simulated smoke agglomerates. *Langmuir*, *4*, 1321–1326.

Mulholland, G. W., & Mountain, R. D. (1999). Coupled dipole calculation of extinction coefficient and polarization ratio for smoke aggregates. *Combustion and Flame*, *119*, 56–68.

Naumann, K.-H., & Bunz, H. (1991). Aerodynamic properties of fractal aerosol particles. *Journal of Aerosol Science*, *22*, S161–S164.

Naumann, K.-H., & Bunz, H. (1992). Computer simulations on the dynamics of fractal aerosols. *Journal of Aerosol Science*, *23*, S361–S364.

Nyeki, S., & Colbeck, I. (1994). The measurement of the fractal dimension of individual in situ soot agglomerates using a modified Millikan cell technique. *Journal of Aerosol Science*, *25*, 75–90.

Okuyama, K., Kousaka, Y., Yamamoto, S., & Hosokawa, T. (1986). Particle loss of aerosols with particle diameters between 6 and 2000 nm in stirred tank. *Journal of Colloid and Interface Science*, *110*, 214–223.

Park, S. H., & Lee, K. W. (2002). Change in particle size distribution of fractal agglomerates during coagulation in the free-molecule regime. *Journal of Colloid and Interface Science*, *246*, 85–91.

Park, S. H., Lee, K. W., Otto, E., & Fissan, H. (1999). The log-normal size distribution theory of Brownian aerosol coagulation for the entire particle size range: Part I—analytical solution using the harmonic mean coagulation kernel. *Journal of Aerosol Science*, *30*, 3–16.

Park, S. H., Xiang, R., & Lee, K. W. (2000). Brownian coagulation of fractal agglomerates: Analytical solution using the log-normal size distribution assumption. *Journal of Colloid and Interface Science*, *231*, 129–135.

Pratsinis, S. (1988). Simultaneous nucleation, condensation, and coagulation in aerosol reactors. *Journal of Colloid and Interface Science*, *124*, 416–427.

Pruppacher, H. R., & Klett, J. D. (1997). *Microphysics of clouds and precipitation*. Dordrecht: Kluwer.

Rogak, S. N., Baltensperger, U., & Flagan, R. C. (1991). Measurement of mass transfer to agglomerate aerosols. *Aerosol Science and Technology*, *14*, 447–458.

Rogak, S. N., & Flagan, R. C. (1989). Stokes drag on self-similar clusters of spheres. *Journal of Colloid and Interface Science*, *134*, 206–218.

Rosner, D. E., & Tandon, P. (1994). Prediction and correlation of accessible area of large multiparticle aggregates. *A.I.Ch.E. Journal*, *40*, 1167–1182.

Saathoff, H. (2003). The AIDA soot aerosol characterization campaign 1999. *Journal of Aerosol Science*, *34*, 1277–1296.

Saathoff, H., Naumann, K.-H., Riemer, N., Kamm, S., Möhler, O., Vogel, B., Vogel, H., & Schurath, U. (2001). The loss of NO_2, HNO_3, NO_3/N_2O_5, and $HO_2/HOONO_2$ on soot aerosol: A chamber and modeling study. *Geophysical Research Letters*, *28*, 1957–1960.

Saathoff, H., Naumann, K.-H., Schnaiter, M., Schöck, W., Möhler, O., Schurath, U., Weingartner, E., Gysel, M., & Baltensperger, U. (2003b) Coating of soot and $(NH_4)_2SO_4$ particles by ozonolysis products of α-pinene. *Journal of Aerosol Science*, *34*, 1297–3602.

Saathoff, H., Naumann, K.-H., Schnaiter, M., Schöck, W., Weingartner, E., Baltensperger, U., Krämer, L., Bozoki, Z., Pöschl, U., Niessner, R., & Schurath, U. (2003c) Carbon mass determinations during the AIDA soot aerosol campaign 1999. *Journal of Aerosol Science*, *34*, 1399–1420.

Schmidt-Ott, A. (1988a). New approaches to in situ characterization of ultrafine agglomerates. *Journal of Aerosol Science*, *19*, 553–563.

Schmidt-Ott, A. (1988b). In situ measurement of the fractal dimensionality of ultrafine aerosol particles. *Applied Physics Letters*, *52*, 954–956.

Schmidt-Ott, A., Baltensperger, U., Gäggeler, H. W., & Jost, D. T. (1990). Scaling behaviour of physical parameters describing agglomerates. *Journal of Aerosol Science*, *21*, 711–717.

Schnaiter, M., Horvath, H., Naumann, K.-H., Saathoff, H., & Schurath, U. (2003) UV-VIS-NIR spectral optical properties of soot and soot-containing aerosols. *Journal of Aerosol Science*, *34*, 1421–1444.

Seigneur, C., Hudischewskyj, A. B., Seinfeld, J. H., Whitby, K. T., Whitby, E. R., Brock, J. R., & Barnes, H. M. (1986). Simulation of aerosol dynamics: A comparative review of mathematical models. *Aerosol Science and Technology*, *5*, 205–222.

Sorensen, C. M. (2001). Light scattering by fractal aggregates: A review. *Aerosol Science and Technology*, *35*, 648–687.

Sorensen, C. M., Cai, J., & Lu, N. (1992). Light-scattering measurements of monomer size, monomers per aggregate, and fractal dimension for soot in flames. *Applied Optics*, *31*, 6547–6557.

Sorensen, C. M., & Feke, G. D. (1996). The morphology of macroscopic soot. *Aerosol Science and Technology*, *25*, 328–337.

Sorensen, C. M., & Roberts, G. C. (1997). The prefactor of fractal aggregates. *Journal of Colloid and Interface Science*, *186*, 447–452.

Tandon, P., & Rosner, D. E. (1999). Monte Carlo simulation of particle aggregation and simultaneous restructuring. *Journal of Colloid and Interface Science*, *213*, 273–286.

van Saarloos, W. (1987). On the hydrodynamic radius of fractal aggregates. *Physica A*, *147*, 280–296.

Vermury, S., Kusters, K. A., & Pratsinis, S. E. (1994). Time lag for attainment of the self-preserving particle size distribution by coagulation. *Journal of Colloid and Interface Science*, *165*, 53–59.

Vermury, S., & Pratsinis, S. E. (1995). Self preserving size distributions of agglomerates. *Journal of Aerosol Science*, *26*, 175–185.

Wang, G. M., & Sorensen, C. M. (1999). Diffusive mobility of fractal aggregates over the entire Knudsen number range. *Physical Review E*, *60*, 3036–3044.

Weingartner, E., Baltensperger, U., & Burtscher, H. (1995). Growth and structural change of combustion aerosol at high relative humidity. *Environment Science & Technology*, *29*, 2982–2986.

Weitz, D. A., & Oliveria, M. (1984). Fractal structures formed by kinetic aggregation of gold colloids. *Physical Review Letters*, *52*, 1433–1436.

Wentzel, M., Gorzawski, H., Naumann, K.-H., Saathoff, H., & Weinbruch, S. (2003). Transmission electron microscopical and aerosol dynamical characterization of soot aerosols. *Journal of Aerosol Science*, *34*, 1347–1370.

Wiltzius, P. (1987). Hydrodynamic behavior of fractal aggregates. *Physical Review Letters*, *58*, 710–713.

Wu, M. K., & Friedlander, S. K. (1993a). Note on the power law equation for fractal-like aerosol agglomerates. *Journal of Colloid and Interface Science*, *159*, 246–248.

Wu, M. K., & Friedlander, S. K. (1993b). Enhanced power law agglomerate growth in the free molecular regime. *Journal of Aerosol Science*, *24*, 273–283.

Xiong, Y., Pratsinis, S. E., & Weimer, A. W. (1992). Modeling the formation of boron carbide particles in an aerosol flow reactor. *A.I.Ch.E. Journal*, *38*, 1685–1692.

Yanwei, Z., & Meriani, S. (1994). Scaling functions for the finite size effect in fractal aggregates. *Journal of Applied Crystallography*, *27*, 782–790.

Zhang, Y., Seigneur, C., Seinfeld, J. S., Jacobson, M. Z., & Binkowski, F. S. (1999). Simulation of aerosol dynamics: A comparative review of algorithms used in air quality models. *Aerosol Science and Technology*, *13*, 487–514.

Ziff, R. M., McGrady, E. D., & Meakin, P. (1985). On the validity of Smoluchowski's equation for cluster–cluster aggregation kinetics. *Journal of Chemical Physics*, *82*, 5269–5274.

Zwanzig, R. (1966). Translational diffusion in polymer solutions. *Journal of Chemical Physics*, *45*, 1858–1859.